Feola et al. EURASIP Journal on Advances in Signal Processing (2015) 2015:28
DOI 10.1186/s13634-015-0207-0

EURASIP Journal on Advances in Signal Processing
a SpringerOpen Journal

RESEARCH Open Access

A new frequency approach for light flicker evaluation in electric power systems

Luigi Feola*, Roberto Langella and Alfredo Testa

Abstract

In this paper, a new analytical estimator for light flicker in frequency domain, which is able to take into account also the frequency components neglected by the classical methods proposed in literature, is proposed. The analytical solutions proposed apply for any generic stationary signal affected by interharmonic distortion. The light flicker analytical estimator proposed is applied to numerous numerical case studies with the goal of showing i) the correctness and the improvements of the analytical approach proposed with respect to the other methods proposed in literature and ii) the accuracy of the results compared to those obtained by means of the classical International Electrotechnical Commission (IEC) flickermeter. The usefulness of the proposed analytical approach is that it can be included in signal processing tools for interharmonic penetration studies for the integration of renewable energy sources in future smart grids.

Keywords: Light flicker; IEC flickermeter; Interharmonic; Distributed energy resources; Power quality; Smart grids

1 Introduction

Light flicker (LF) phenomenon is still considered one of the most important power quality (PQ) problems due to its ability to be directly perceived by customers, producing complaints from them.

LF is caused by the modulation of the supply fundamental voltage, which produces modulated light emissions whose severity, in terms of annoying effects on humans, depends on modulation amplitudes and frequencies as well as on lamp technologies [1]. LF is commonly measured by means of the International Electrotechnical Commission (IEC) flickermeter [2] that, for historical reasons, was designed and tested only with reference to voltage amplitude modulation (AM), which was the first source of LF identified and referring only to 60-W incandescent bulbs, which were the most diffused lamps all over the word at that time.

Today, incandescent lamps are going to be banned, in particular in Europe, Australia and North America, but the IEC flickermeter is still the only instrument used also because international standards are based on it.

The main drawbacks of the IEC flickermeter are as follows: i) it is based on the incandescent bulb model; ii) it requires 10 min of time domain signals to give the short-term flicker sensation index output, P_{st}; and iii) the output data cannot be used to study LF propagation effects in distribution and transmission networks.

Basic literature demonstrates the perfect equivalence of amplitude modulation to the summation of interharmonic tones of proper amplitudes and phase angles superimposed to the fundamental [3].

Starting from the beginning of the last decade, several papers aimed to model the IEC flickermeter in the frequency domain have been written [4-13]. Some of them [4,7,10,11] are pure frequency domain methods. Some others [6,9,12] are hybrid time-frequency domain methods.

Mayordomo et al. obtained very accurate analytical formulas that were applied to the voltages of DC and AC electrical arc furnace (EAF) measurements. In [13], the analytical formulas have been used to evaluate the propagation in the network of flicker produced by rapidly varying loads. In [11], a spectral decomposition-based approach is proposed to estimate LF caused by EAFs where

* Correspondence: luigi.feola@unina2.it
Department of Industrial and Information Engineering, Second University of Naples, DIII-SUN, Via Roma, 29, 81031 Aversa, Caserta, Italy

the system frequency deviates significantly due to the EAF operation. Both methods start from the discrete Fourier transform (DFT) performed over 200 ms, which is perfectly compatible with the IEC Standard 61000-4-7 [14] that defines harmonic and interharmonic measurement techniques.

All of the above-mentioned methods are based on simplified assumptions essentially based on the concept that, due to the design specifications of the filters of the IEC flickermeter, the interharmonic components below 15 Hz and above 85 Hz can be neglected, with reference to 50 Hz systems. This assumption is demonstrated to be valid when the interharmonic source is an EAF which mainly produces modulation of the fundamental voltage in the frequency range from 0 to 20 Hz, that is to say modulations produced by interharmonics in the frequency range from 20 to 80 Hz. Recent studies have demonstrated that modern distributed energy resources, in particular wind turbines, are able to produce interharmonics in a wide range of frequency from DC to some kilohertz [15]. Moreover, in [16-18], it was demonstrated that interharmonic components produced by adjustable speed drives can cover all the frequency range from DC.

In this paper, the above-mentioned simplified assumption is overcome, leading to analytical solutions, of different complexities, able to take into account also the frequency components neglected by the classical methods. The analytical solutions proposed apply for any generic stationary signal affected by interharmonic distortion. The LF analytical estimator proposed is applied to numerous numerical case studies with the goal of showing i) the correctness and the improvements of the analytical approach proposed with respect to the other methods proposed in literature and ii) the accuracy of the results compared to those obtained by means of the classical IEC flickermeter. The usefulness of the proposed analytical approach is that it can be included in signal processing tools for interharmonic penetration studies for the integration of renewable energy sources in future smart grids.

2 Analytical assessment of IEC flickermeter response due to interharmonics

In this section, the behaviour of the IEC flickermeter in terms of instantaneous flicker sensation (PU), that is the output of the block 4 of the IEC flickermeter (Figure 1), is analytically assessed.

The analytical solutions proposed apply for any generic stationary signal affected by interharmonic distortion. The generic signal is decomposed into N interharmonic pairs. Each pair is constituted of two tones in symmetrical frequency positions with respect to the fundamental frequency. Moreover, each of two components of the pair has generic amplitude and generic phase angle. Obviously, the case of single interharmonic components can be easily obtained assuming the amplitude of one of the two components of the pair equal to zero.

Here, explicit reference is made to 50-Hz systems, but the considerations developed may also be applied to 60-Hz systems by changing the constants and parameters.

2.1 Single pair

A normalized voltage with a couple of superimposed interharmonic tones ($N = 1$) in symmetrical angular frequency positions (lower and upper) with respect to the fundamental signal ($\omega_{1\_L} = \omega_1 - \Delta\omega_1$ and $\omega_{1\_U} = \omega_1 + \Delta\omega_1$) can be expressed as:

$$\begin{aligned}\frac{u(t)}{\hat{u}} = {} & a_0 cos(\omega_1 t + \varphi_1) \\ & + a_{1\_L} cos[(\omega_1 - \Delta\omega_1)t + \varphi_{1\_L}] \\ & + a_{1\_U} cos[(\omega_1 + \Delta\omega_1)t + \varphi_{1\_U}],\end{aligned} \quad (1)$$

with $\hat{u}$ representing the half cycle rms value processed through a first-order filter with a time constant of 27.3 s; a_0, ω_1 and φ_1, respectively, representing the relative amplitude, the angular frequency and the phase angle of the fundamental tone; a_{1_L} and a_{1_U} representing the relative amplitudes of the interharmonic tones and φ_{1_L} and φ_{2_L} representing their phase angles, respectively.

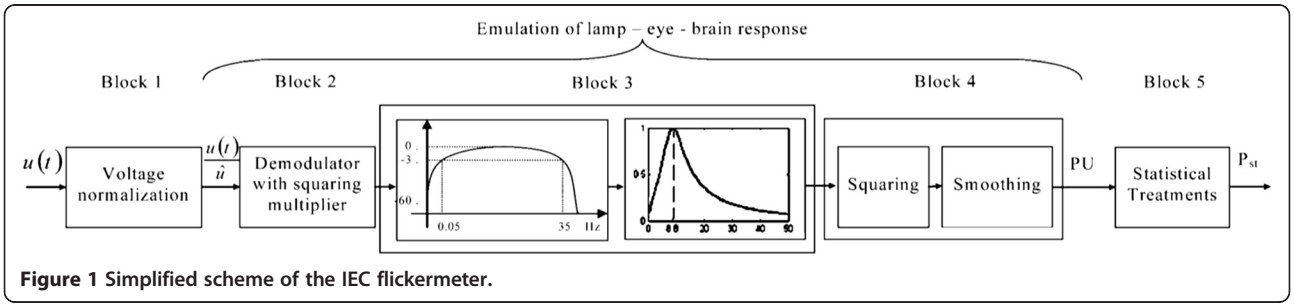

Figure 1 Simplified scheme of the IEC flickermeter.

The squaring of (1) (block 2 in Figure 1) yields a demodulated signal that is very close to the luminous flux Φ:

$$\begin{aligned}\left[\frac{u(t)}{\hat{u}}\right]^2 &= \frac{1}{2}\left(a_0^2 + a_{1\_L}^2 + a_{1\_U}^2\right)\\ &+\frac{1}{2}\left\{a_0^2\cos(2\omega_1 t + 2\varphi_1) + a_{1\_L}^2\cos[2(\omega_1 - \Delta\omega_1)t + 2\varphi_{1\_L}]\right.\\ &\left.+a_{1\_U}^2\cos[2(\omega_1 + \Delta\omega_1)t + 2\varphi_{1\_U}]\right\}\\ &+a_0 a_{1\_L}\{\cos(\Delta\omega_1 t - \varphi_{1\_L} + \varphi_1) + \cos[(2\omega_1 - \Delta\omega_1)t + \varphi_{1\_L} + \varphi_1]\}\\ &+a_0 a_{1\_U}\{\cos(\Delta\omega_1 t + \varphi_{1\_U} + \varphi_1) + \cos[(2\omega_1 + \Delta\omega_1)t + \varphi_{1\_U} + \varphi_1]\}\\ &+a_{1\_L}a_{1\_U}[\cos(2\Delta\omega_1 t - \varphi_{1\_L} + \varphi_{1\_U}) + \cos(2\omega_1 t + \varphi_{1\_L} + \varphi_{1\_U})],\end{aligned} \tag{2}$$

Block 3 is composed of a cascade of two filters. The first is used to eliminate the DC component and the component at twice the fundamental frequency present at the output of the demodulator. This filter is composed of a cascade of a high-pass filter (HPF) of first order with a cutoff frequency of 0.05 Hz and a Butterworth low-pass filter (LPF) of the sixth order with a cutoff frequency of 35 Hz for 230 V/50 Hz systems. The second is used to weigh the voltage fluctuation according to the lamp-eye-brain sensitivity. The transfer functions and the Bode diagrams for these filters are reported in (3) and (4) and in Figure 2 together with their product $G(s) = X(s)\,F(s)$.

$$X(s) = \frac{s}{s + \omega_{\mathrm{HPF}}}\frac{n_0}{s^6 + d_5 s^5 + d_4 s^4 + d_3 s^3 + d_2 s^2 + d_1 s + d_0}, \tag{3}$$

$$F(s) = \frac{k\omega_1 s}{s^2 + 2\lambda s + \omega_1^2}\frac{1 + s/\omega_2}{(1 + s/\omega_3)(1 + s/\omega_4)}, \tag{4}$$

being the coefficient of $X(s)$ and $F(s)$ shown in Table 1 and in Table 2, respectively [2].

Under the hypothesis that block 3 gates the DC component and all the components at a frequency certainly higher than 100 Hz (frequencies greater than the cutoff frequency of 35 Hz) and considering $G(s) = X(s)\,F(s)$ the output of the block 3 is:

$$\begin{aligned}\Delta\Phi \cong H\Big\{ &|G_{\Delta\omega_1}|a_0 a_{1\_L}\cos(\Delta\omega_1 t - \varphi_{1\_L} + \varphi_1 + \angle G_{\Delta\omega_1})\\ &+ |G_{\Delta\omega_1}|a_0 a_{1\_U}\cos(\Delta\omega_1 t + \varphi_{1\_U} - \varphi_1 + \angle G_{\Delta\omega_1})\\ &+ |G_{2\Delta\omega_1}|a_{1\_L}a_{1\_U}\cos(2\Delta\omega_1 t - \varphi_{1\_L} + \varphi_{1\_U} + \angle G_{2\Delta\omega_1})\\ &+ |G_{2\omega_1 - \Delta\omega_1}|a_0 a_{1\_L}\cos[(2\omega_1 - \Delta\omega_1)t + \varphi_{1\_L} + \varphi_1 + \angle G_{2\omega_1 - \Delta\omega_1}]\\ &+ |G_{2\omega_1 - 2\Delta\omega_1}|\frac{a_{1\_L}^2}{2}\cos[2(\omega_1 - \Delta\omega_1)t + 2\varphi_{1\_L} + \angle G_{2\omega_1 - 2\Delta\omega}]\Big\},\end{aligned} \tag{5}$$

where $H = \sqrt{1238400}$ is a gain factor related to the normalization of the weighting curve, and four different magnitude and phase gains $G_{\Delta\omega_1}, G_{2\Delta\omega_1}, G_{2\omega_1 - \Delta\omega_1}$ and $G_{2\omega_1 - 2\Delta\omega_1}$ are introduced for the five components depending on their angular frequency distances.

Block 4 of the flickermeter squares and filters the input signal. The filtering is obtained by means of a low-pass filter with a cutoff frequency of 0.5305 Hz and transfer function equal to:

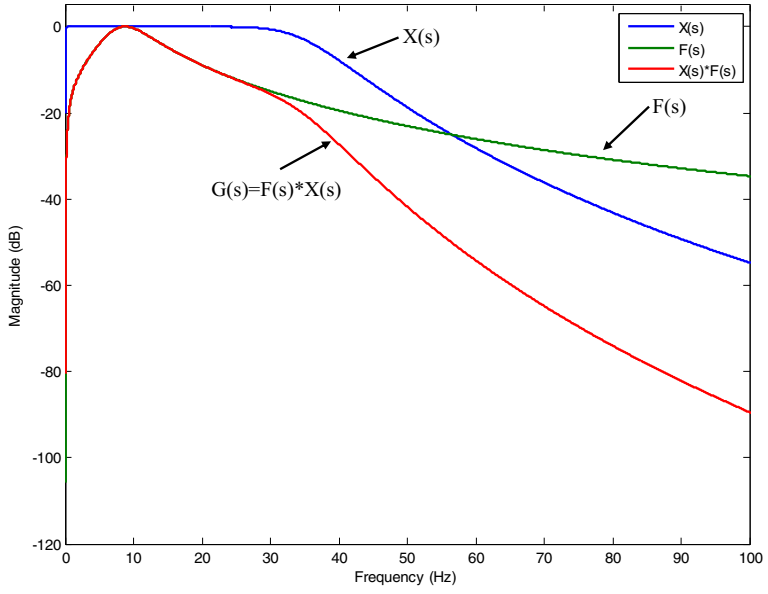

Figure 2 Magnitude Bode diagrams of block 3 filters.

Table 1 Design parameter of *X*(*s*)

ωHPF	n_0	d_0	d_1	d_2	d_3	d_4	d_5
$2\pi 0.05$	$1.13\ 10^{14}$	$1.13\ 10^{14}$	$1.99\ 10^{12}$	$1.75\ 10^{10}$	$9.72\ 10^{7}$	$3.61\ 10^{5}$	849.7

$$Y(s) = \frac{2\pi 0.5305}{s + 2\pi 0.5305}. \tag{6}$$

This filter has the goal to attenuate all the sinusoidal components, leaving the continuous component unaffected. Although the bandwidth of the filter is very narrow, not all the sinusoidal components may be void. For this reason, the instantaneous flicker sensation due to the single interharmonic pair can be written as:

$$\mathrm{PU}_1(t) = \mathrm{PU}_{1\_\mathrm{DC}} + \mathrm{PU}_{1\_\mathrm{AC}}(t), \tag{7}$$

where $\mathrm{PU}_{1\_\mathrm{DC}}$ and $\mathrm{PU}_{1\_\mathrm{AC}}(t)$ are the DC and the residual AC component of the instantaneous flicker sensation, respectively.

With reference only to the DC component of PU_1 and applying at the block 4 the signal (5), it is possible to demonstrate that:

$$\mathrm{PU}_{1\_\mathrm{DC}} = \mathrm{PU}_{1\_\mathrm{DC1}} + \mathrm{PU}_{1\_\mathrm{DC2}}, \tag{8}$$

where $\mathrm{PU}_{1\_\mathrm{DC1}}$ and $\mathrm{PU}_{1\_\mathrm{DC2}}$ are equal, respectively, to:

$$\mathrm{PU}_{1\_\mathrm{DC1}} \cong \frac{1}{2}H^2|G_{\Delta\omega_1}|^2 a_0^2 \times \left[a_{1\_\mathrm{L}}^2 + a_{1\_\mathrm{U}}^2 + 2a_{1\_\mathrm{L}}a_{1\_\mathrm{U}}\cos(\varphi_{1\_\mathrm{L}} + \varphi_{1\_U} - 2\varphi_1)\right], \tag{9}$$

$$\mathrm{PU}_{1\_\mathrm{DC2}} \cong \frac{1}{2}H^2\left[|G_{2\Delta\omega_1}|^2 a_{1\_\mathrm{L}}^2 a_{1\_\mathrm{U}}^2 + |G_{2\omega_1+\Delta\omega_1}|^2 a_0^2 a_{1\_\mathrm{L}}^2 + |G_{2\omega_1+2\Delta\omega_1}|^2 \frac{a_{1\_\mathrm{L}}^4}{4}\right]. \tag{10}$$

As it will be shown in a more comprehensive manner in the following sections, the first component (9) assumes prevalent values for all the values of $\Delta\omega_1$ while the second (10) assumes values increasingly larger how close is the frequency of the lower interharmonic tone to zero.

It is worth noting that (9) corresponds to the analogous expressions reported in [7] and in [10]. The difference is that in cited references, the filter $X(s)$ was considered ideal, that is to say that $G(s) = X(s)F(s) = F(s)$; so (9) considers the red curve of Figure 2 instead of the green one considered in [7] and in [10].

Table 2 Design parameter of *F*(*s*)

k	λ	ω_1	ω_2	ω_3	ω_4
1.74802	2π 4.05981	2π 9.15494	2π 2.27979	2π 1.22535	2π 21.9

With reference only to the residual AC component of PU_1 and applying at the block 4 the signal (5), it is possible to demonstrate that:

$$\mathrm{PU}_{1\_\mathrm{AC}}(t) = \mathrm{PU}_{1\_\mathrm{AC1}}(t) + \mathrm{PU}_{1\_\mathrm{AC2}}(t), \tag{11}$$

where $\mathrm{PU}_{1\_\mathrm{AC1}}$ and $\mathrm{PU}_{1\_\mathrm{AC2}}$, considering only the component of major interest, are equal, respectively, to:

$$\mathrm{PU}_{1\_\mathrm{AC1}}(t) \cong \mathrm{PU}_{1\_\mathrm{AC1}\_\Delta\omega_1}(t) + \mathrm{PU}_{1\_\mathrm{AC1}\_2\Delta\omega_1}(t) + \mathrm{PU}_{1\_\mathrm{AC1}\_3\Delta\omega_1}(t) + \mathrm{PU}_{1\_\mathrm{AC1}\_4\Delta\omega_1}(t), \tag{12}$$

$$\mathrm{PU}_{1\_\mathrm{AC2}}(t) \cong \mathrm{PU}_{1\_\mathrm{AC2}\_(2\omega_1-2\Delta\omega_1)}(t) + \mathrm{PU}_{1\_\mathrm{AC2}\_(4\omega_1-4\Delta\omega_1)}(t). \tag{13}$$

$\mathrm{PU}_{1\_\mathrm{AC1}}$ and $\mathrm{PU}_{1\_\mathrm{AC2}}$ are oscillating components due to the summation of sinusoidal signals with different angular frequencies (the angular frequency of each summand is indicated in the subscript). In particular, $\mathrm{PU}_{1\_\mathrm{AC1}}$ assumes higher values how close $\Delta\omega_1$ is to zero, while $\mathrm{PU}_{1\_\mathrm{AC2}}$ assumes higher values how close $\Delta\omega_1$ is to the fundamental angular frequency.

For the sake of brevity, the analytical assessment of the summands of (12) and (13) are reported extensively in Appendix A.

2.2 Two pairs

A normalized voltage with two pairs of superimposed interharmonic tones in symmetrical frequency positions ($\Delta\omega_1$ and $\Delta\omega_2$) with respect to the fundamental signal can be expressed as:

$$\begin{aligned} u(t)\hat{u} = {} & a_0\cos(\omega_1 t + \varphi_1) + a_{1\_\mathrm{L}}\cos[(\omega_1 - \Delta\omega_1)t + \varphi_{1\_\mathrm{L}}] \\ & + a_{1\_\mathrm{U}}\cos[(\omega_1 + \Delta\omega_1)t + \varphi_{1\_\mathrm{U}}] \\ & + a_{2\_\mathrm{L}}\cos[(\omega_1 - \Delta\omega_2)t + \varphi_{2\_\mathrm{L}}] \\ & + a_{2\_\mathrm{U}}\cos[(\omega_1 + \Delta\omega_2)t + \varphi_{2\_\mathrm{U}}], \end{aligned} \tag{14}$$

where a_{1_L} and a_{1_U} and φ_{1_L} and φ_{1_U} represent the relative amplitudes and the phase angles of the first interharmonic pair, respectively, and a_{2_L} and a_{2_U} and φ_{2_L} and φ_{2_U} of the second interharmonic pair, respectively.

Using the same procedure used for the single pair of interharmonic tones (shown in Section 2.1) and neglecting the effect on the AC component of the instantaneous flicker sensation of the interaction between the two interharmonic pairs, it is possible to demonstrate that:

$$\begin{aligned}\mathrm{PU}_{1+2} &= \mathrm{PU}_1 + \mathrm{PU}_2 + \mathrm{PU}_{12\_\mathrm{DC}} = \mathrm{PU}_{1\_\mathrm{DC}} + \mathrm{PU}_{1\_\mathrm{AC}} \\ &\quad + \mathrm{PU}_{2\_\mathrm{DC}} + \mathrm{PU}_{2\_\mathrm{AC}} + \mathrm{PU}_{12\_\mathrm{DC}} \\ &= (\mathrm{PU}_{1\_\mathrm{DC}} + \mathrm{PU}_{2\_\mathrm{DC}} + \mathrm{PU}_{12\_\mathrm{DC}}) \\ &\quad + (\mathrm{PU}_{1\_\mathrm{AC}} + \mathrm{PU}_{2\_\mathrm{AC}}) \\ &= \mathrm{PU}_{1+2\_\mathrm{DC}} + \mathrm{PU}_{1+2\_\mathrm{AC}},\end{aligned} \tag{15}$$

where PU_1 and PU_2 are obtained by means of (7) for the interharmonic pair tones and $\mathrm{PU}_{12\_\mathrm{DC}}$ is the DC component of instantaneous flicker sensation due to the interaction between the two interharmonic pairs. For sake of brevity, the analytical assessment of $\mathrm{PU}_{12\_\mathrm{DC}}$ is reported in Appendix B. Again, as in (7), two different components, one DC ($\mathrm{PU}_{1+2\_\mathrm{DC}}$) and the other AC ($\mathrm{PU}_{1+2\_\mathrm{AC}}$), are defined.

From the previous formulas, it should be noted that in case of two interharmonic couples superimposed to the fundamental signal, the PU is not only due to the sum of the contributions to the instantaneous flicker sensation of the single interharmonic pair, but there is also a component due to the combination effect of the interharmonic pairs. The entity of this effect will be evaluated in the following sections.

2.3 *N* pairs

Starting from the analytical assessments of Section 2.2, it is possible to generalize the analytical assessment to the case of N pairs of interharmonic tones. In fact, from (15), it is possible to obtain:

$$\begin{aligned}\mathrm{PU}_{\mathrm{TOT}} &= \sum_{j=0}^{\infty} \mathrm{PU}_j + \sum_{j=0}^{\infty} \sum_{k=j+1}^{\infty} \mathrm{PU}_{kj\_\mathrm{DC}} \\ &= \sum_{j=0}^{\infty} \left(\mathrm{PU}_{j\_\mathrm{DC}} + \mathrm{PU}_{j\_\mathrm{AC}}\right) + \sum_{j=0}^{\infty} \sum_{k=j+1}^{\infty} \mathrm{PU}_{kj\_\mathrm{DC}} \\ &= \sum_{j=0}^{\infty} \left(\mathrm{PU}_{j\_\mathrm{DC1}} + \sum_{k=j+1}^{\infty} \mathrm{PU}_{kj\_\mathrm{DC}} \right) + \sum_{j=0}^{\infty} \mathrm{PU}_{j\_\mathrm{AC}} \\ &= \mathrm{PU}_{\mathrm{TOT}\_\mathrm{DC}} + \mathrm{PU}_{\mathrm{TOT}\_\mathrm{AC}},\end{aligned} \tag{16}$$

where $\mathrm{PU}_{\mathrm{TOT\_DC}}$ and $\mathrm{PU}_{\mathrm{TOT\_AC}}$ are the DC and the AC components, respectively, of the instantaneous flicker sensation due to N symmetric interharmonic pairs superimposed to the fundamental signal.

3 Numerical case studies

In this section, different numerical case studies are shown to validate the analytical assessment presented in Section 2. The results obtained by a numerical implementation of the IEC flickermeter (according with the standard IEC 61000-4-15) and the results obtained by the formulas of the analytical flickermeter presented in this paper, both implemented in MATLAB, are compared. The block diagram of the numerical case studies is shown in Figure 3.

The steps performed to obtain the results of each numerical case study are as follows:

1. A time domain signal with a length of 10 min with different characteristics, according with the case study, is generated.
2. The signal is analysed by means of the IEC flickermeter, which returns both the reference of the instantaneous flicker sensation and of the short-term flicker severity value, $\mathrm{PU}_{\mathrm{ref}}$ and $P_{\mathrm{st\_ref}}$, respectively.
3. A DFT is performed only on the Fourier period of the signal-generated [1] since the signal is stationary in terms of fundamental and interharmonic signals in all the 10 min.
4. The output of the DFT is analysed by means of the analytical formulas of Section 2, according with the case study, to obtain the value of instantaneous flicker sensation (PU).
5. The instantaneous flicker sensation is used as input to the statistical evaluation (like that described in the Standard IEC 61000-4-15) to obtain the short-term flicker severity (P_{st}).
6. The values of $\mathrm{PU}_{\mathrm{ref}}$, $P_{\mathrm{st\_ref}}$, PU and P_{st} so obtained have been post-processed to calculate the error of the analytical estimation.

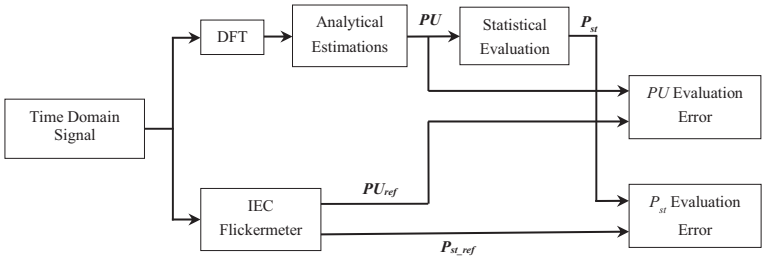

Figure 3 Block diagram of the numerical case studies.

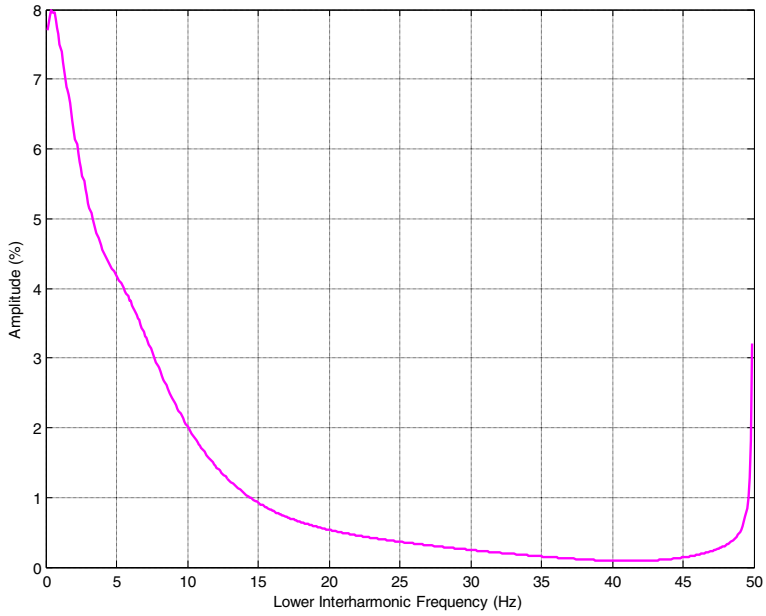

Figure 4 Amplitudes of pairs of symmetric interharmonics causing unitary P_{st} versus the pair lower interharmonic frequency.

3.1 Single pair producing AM

The interharmonic pairs have modulation frequencies varying between 0.1 and 49.9 Hz with steps of 0.1 Hz. For each modulation frequency, the amplitude of the pair taken from Figure 4, where the interharmonic amplitudes of pairs of symmetric interharmonic tones superimposed to the fundamental causing a P_{st} equal to 1 versus the lower interharmonic frequency of the pair, is shown. Furthermore, it should be noted that since the Fourier period of the signal generated is 10 s, a DFT with a spectral resolution of 0.1 Hz is used.

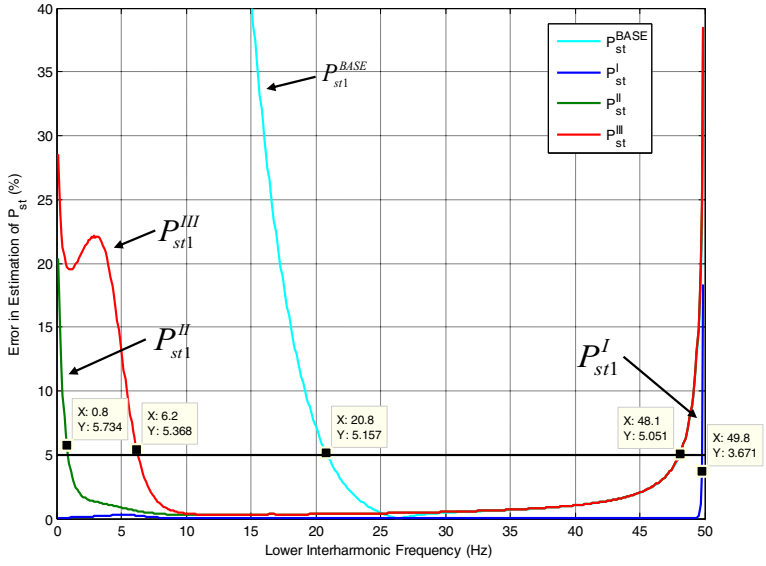

Figure 5 Percentage errors in estimation of P_{st} versus lower frequency of symmetric interharmonic pairs producing AM and unitary P_{st}. P^{BASE}_{st1}, P^{I}_{st1}, P^{II}_{st1} and P^{III}_{st1} indicate the short-term flicker severity index considering, respectively, the analytical estimation proposed in [7] (cyan), the AC and the DC component of PU_1 (17) (blue), only the DC component of PU_1 (18) (green) and only the PU_{1_DC1} component of PU_1 (19) (red).

Three different analytical estimations of the instantaneous Flicker sensation, with decreasing complexity, have been considered:

$$\text{I)}\ \mathrm{PU}_1^{\mathrm{I}} = \mathrm{PU}_1 = \mathrm{PU}_{1\_\mathrm{DC1}} + \mathrm{PU}_{1\_\mathrm{DC2}} + \mathrm{PU}_{1\_\mathrm{AC}}; \quad (17)$$

$$\text{II)}\ \mathrm{PU}_1^{\mathrm{II}} = \mathrm{PU}_{1\_\mathrm{DC}} = \mathrm{PU}_{1\_\mathrm{DC1}} + \mathrm{PU}_{1\_\mathrm{DC2}}; \quad (18)$$

$$\text{III)}\ \mathrm{PU}_1^{\mathrm{III}} = \mathrm{PU}_{1\_\mathrm{DC1}}. \quad (19)$$

Obviously, the corresponding values of $P_{\mathrm{st1}}^{\mathrm{I}}, P_{\mathrm{st1}}^{\mathrm{II}}$ and $P_{\mathrm{st1}}^{\mathrm{III}}$ have been calculated. Moreover, the results obtained implementing the analytical assessment proposed in [7] are reported and referred to as $P_{\mathrm{st1}}^{\mathrm{BASE}}$.

In Figure 5, the percentage errors (- $P_{\mathrm{st1}}^{\mathrm{BASE}}$ - cyan curve, - $\mathrm{PU}_1^{\mathrm{I}}$ - blue curve, - $\mathrm{PU}_1^{\mathrm{II}}$ - green curve, - $\mathrm{PU}_1^{\mathrm{III}}$ - red curve) versus the lower interharmonic frequency of the symmetric interharmonic pair are shown.

From Figure 5, it is possible to observe the following:

- The blue curve $\left(P_{\mathrm{st1}}^{\mathrm{I}}\right)$, in all the frequency range analysed, gives the best results and only for the pair with the frequency of 49.9 Hz shows an error greater than 5% (black line). For this frequency, the error is caused mainly by the transient behaviour of the filters contained in the IEC flickermeter, which becomes non-negligible for interharmonic frequencies very close to the fundamental. This transient behaviour is not taken into account by pure frequency domain methods differently from hybrid methods [12].
- The green curve $\left(P_{\mathrm{st1}}^{\mathrm{II}}\right)$ and the red curve $\left(P_{\mathrm{st1}}^{\mathrm{III}}\right)$ are virtually indistinguishable for frequencies greater than 15 Hz. Below this frequency (as mentioned in Section 2), the impact of $\mathrm{PU}_{1\_\mathrm{DC2}}$ on the total value of PU_1 is non-negligible, and for this reason, in this frequency range, the error committed by the analytical estimation $P_{\mathrm{st1}}^{\mathrm{II}}$ is less than that produced by $P_{\mathrm{st1}}^{\mathrm{III}}$.
- The $P_{\mathrm{st1}}^{\mathrm{II}}$ estimation makes an error greater than 5% (black line) for the pairs with frequencies higher than 48 Hz and lower than 0.8 Hz. The reason of these errors (in addition to the previously mentioned transient behaviour of the IEC flickermeter for interharmonic frequencies very close to the fundamental) is due to the AC component of PU_1, which is more consistent for interharmonic tones with $\Delta\omega_1$ both close to the fundamental frequency or close to zero.
- The $P_{\mathrm{st1}}^{\mathrm{III}}$ estimation makes an error greater than 5% (black line) for frequencies lower than 6.2 Hz and higher than 48 Hz. The reasons of the different trend of the red curve with respect to the other two curves are the same as the ones mentioned in the previous point.
- The $P_{\mathrm{st1}}^{\mathrm{BASE}}$ (cyan curve) makes an error almost equal to the $P_{\mathrm{st1}}^{\mathrm{II}}$ and the $P_{\mathrm{st1}}^{\mathrm{III}}$ for frequencies higher than 25 Hz, but for lower frequencies, as a result of the simplifying assumptions, the error diverges, rapidly reaching the 40% already for a frequency of 15 Hz.

3.2 Two pairs producing AM

The amplitude of the single pair of interharmonic tones has been chosen to produce singly a P_{st} equal to 1 (Figure 4). The frequency modulation of the two pairs, which are defined $\Delta\omega_1$ and $\Delta\omega_2$ in (14), has been chosen to vary between 1 and 49 Hz, with steps of 1 Hz, and all their possible combinations have been evaluated. Since the Fourier period of the input signal is equal to 1 s, a DFT with a spectral resolution of 1 Hz is used.

Three different analytical estimations of the cumulative P_{st} ($P_{\mathrm{st1+2}}$) have been considered, all based on (15):

$$\text{I)}\ \mathrm{PU}_{1+2}^{\mathrm{I}} = \mathrm{PU}_{1+2} = \mathrm{PU}_{1+2\_\mathrm{DC}} + \mathrm{PU}_{1+2\_\mathrm{AC}}. \quad (20)$$

$$\text{II)}\ \mathrm{PU}_{1+2}^{\mathrm{II}} = \mathrm{PU}_{1+2\_\mathrm{DC}}. \quad (21)$$

$$\text{III)}\ \mathrm{PU}_{1+2}^{\mathrm{III}} = \mathrm{PU}_1 + \mathrm{PU}_2. \quad (22)$$

Obviously, the corresponding values of $P_{\mathrm{st1+2}}^{\mathrm{I}}, P_{\mathrm{st1+2}}^{\mathrm{II}}$ and $P_{\mathrm{st1+2}}^{\mathrm{III}}$ have been calculated. Moreover, the results obtained implementing the analytical assessment proposed in [7] are reported and referred to as $P_{\mathrm{st1+2}}^{\mathrm{BASE}}$.

In Figures 6, 7, 8 and 9, the percentage errors for the analytical estimation, $\mathrm{PU}_{1+2}^{\mathrm{I}}, \mathrm{PU}_{1+2}^{\mathrm{II}}, PU_{1+2}^{\mathrm{III}}$ and $P_{\mathrm{st1+2}}^{\mathrm{BASE}}$ are shown.

From these figures, it should be noted that

- The x-axis and the y-axis represent the frequency of lower interharmonic tone of the first and of the second interharmonic pair, respectively.
- The most complete analytical estimation $P_{\mathrm{st1+2}}^{\mathrm{I}}$ (Figure 6), for the most part of the cases analysed, makes a mistake lower than 5% (light green squares). The cases with an error greater than the 5% occur essentially when the interaction between the two interharmonic pairs produces one or more oscillating component of the PU_{1+2} with an angular frequency that the filter $Y(s)$ (6) is not able to eliminate, which is not evaluated analytically.

These events occur when

i) $\Delta\omega_1 \approx \Delta\omega_2$ (main diagonal);
ii) Both the lower interharmonic tones of the two pairs are lower than 5 Hz (in the top left corner);

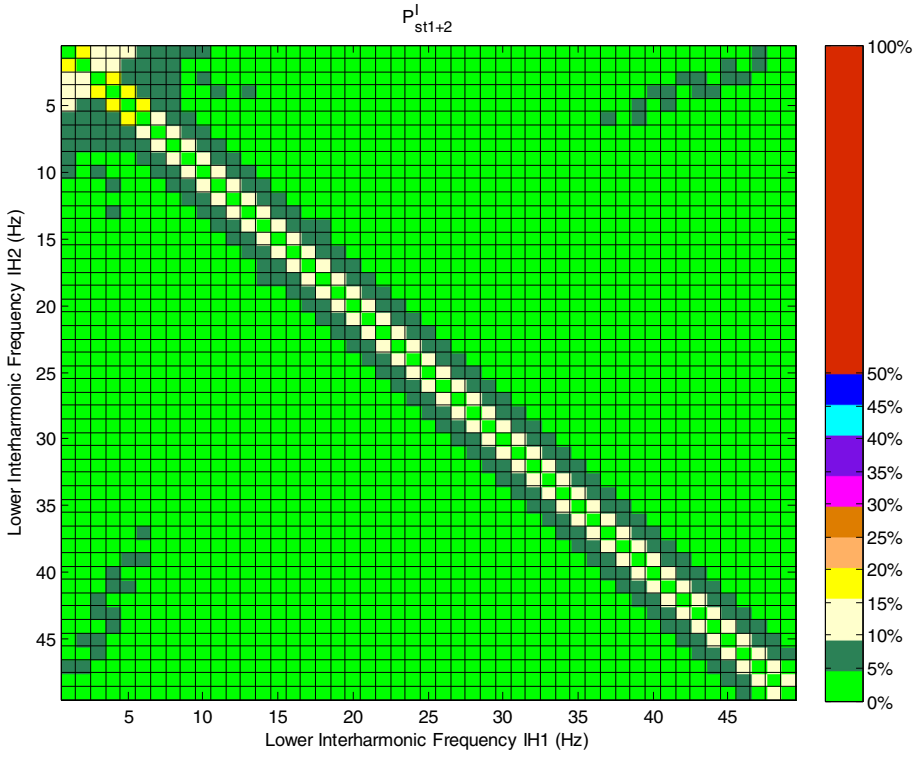

Figure 6 Percentage errors in the evaluation of P_{st} of two pairs of interharmonic tones producing AM for P^{I}_{st1+2} (20).

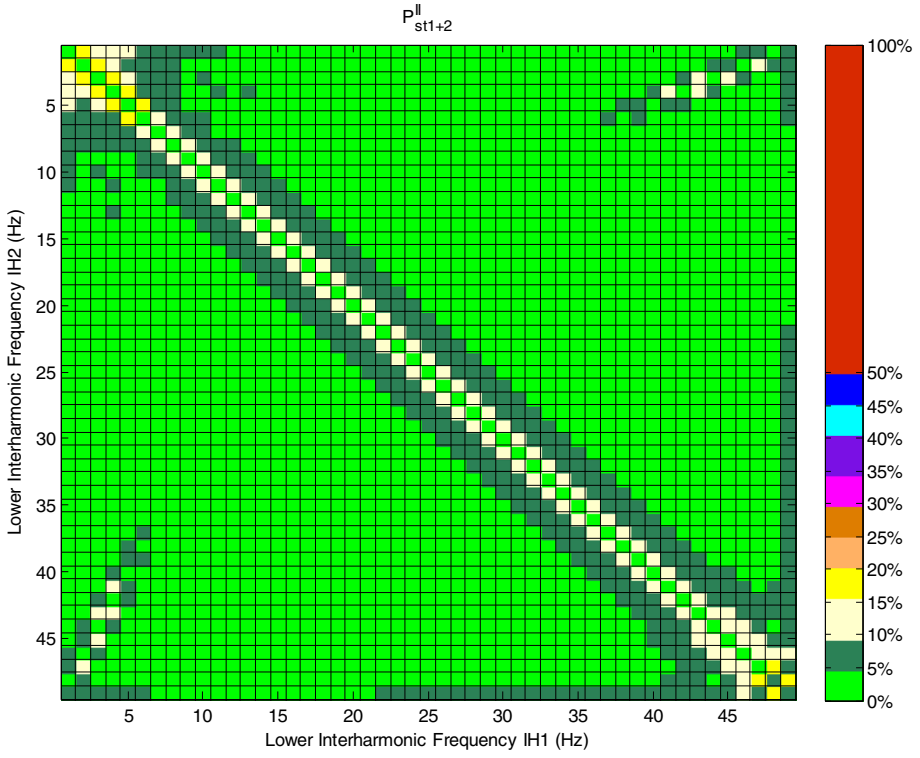

Figure 7 Percentage errors in the evaluation of P_{st} of two pairs of interharmonic tones producing AM for PU^{II}_{1+2} (21).

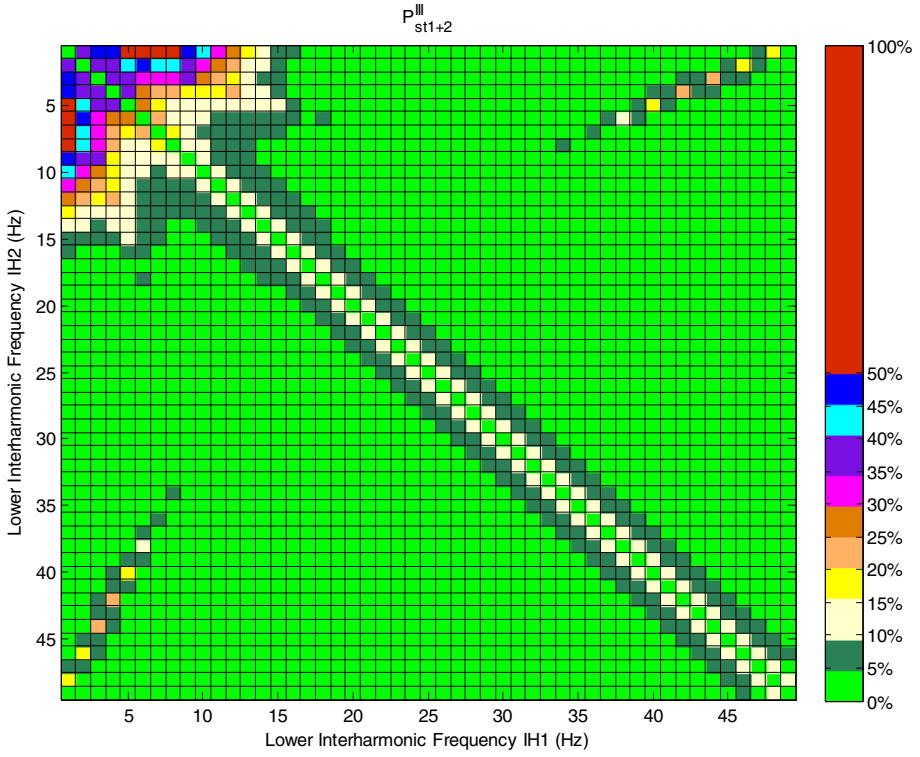

Figure 8 Percentage errors in the evaluation of P_{st} of two pairs of interharmonic tones producing AM for PU^{III}_{1+2} (22).

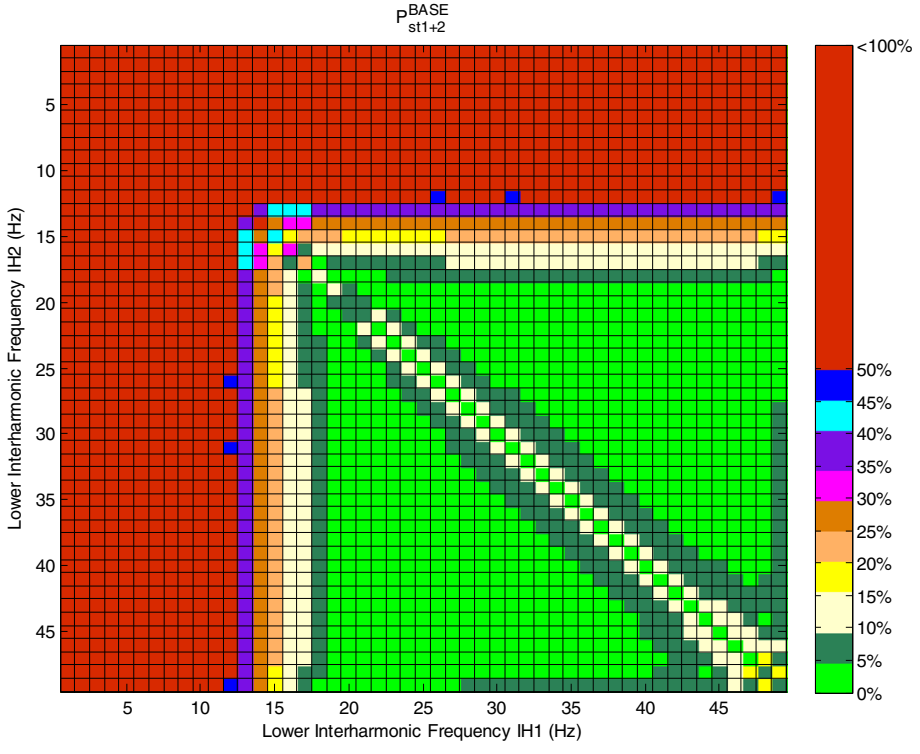

Figure 9 Percentage errors in the evaluation of P_{st} of two pairs of interharmonic tones producing AM for P^{BASE}_{st1+2}.

iii) $\Delta\omega_1 \approx 2(\omega_1 - \Delta\omega_2)$ (in the top right corner);
iv) $\Delta\omega_2 \approx 2(\omega_1 - \Delta\omega_1)$ (in the bottom left corner).

- Comparing the results obtained for $P^{\mathrm{I}}_{\mathrm{st1+2}}$ (Figure 6) and for $P^{\mathrm{II}}_{\mathrm{st1+2}}$ (Figure 7), it should be noted that neglecting the effects of the AC components produced by the single interharmonic pair increases the number of non-light green squares when

i) $\Delta\omega_1 \approx \Delta\omega_2$ (main diagonal);
ii) $\Delta\omega_1 \approx 2(\omega_1 - \Delta\omega_2)$ (in the top right corner) and when $\Delta\omega_2 \approx 2(\omega_1 - \Delta\omega_1)$ (in the bottom left corner);
iii) $\Delta\omega_1 = 1$ (last column to the right) and when $\Delta\omega_2 = 1$ (last column to the bottom).

- Comparing the results obtained for $P^{\mathrm{I}}_{\mathrm{st1+2}}$ (Figure 6) and for $P^{\mathrm{III}}_{\mathrm{st1+2}}$ (Figure 8), it should be noted that neglecting the effects of the interactions between the two interharmonic pairs on the DC component of the PU_{1+2} are present with a non-negligible entity when

i) Both the pairs have the lower interharmonic tone frequency lower than 15 Hz (in the top left corner);
ii) $\Delta\omega_1 = 2(\omega_1 - \Delta\omega_2)$ (in the top right corner) or when $\Delta\omega_2 \approx 2(\omega_1 - \Delta\omega_1)$ (in the bottom left corner).

- In similar mode to the case of an interharmonic pair shown in Figure 5, the analytical assessment $P^{\mathrm{BASE}}_{\mathrm{st1+2}}$ (Figure 9) makes errors very high (sometimes even more than 100%) when one or both the pairs have the lower interharmonic tone with frequencies lower than 20 Hz.
- Finally, it is worthwhile to note that from the implementation point of view on a general PQ instrument, the proposed analytical approach requires only some manipulations, of different complexities depending on the level of approximation desired (see (20), (21) and (22)), of the spectra which are already evaluated by the PQ instrument for the harmonic and interharmonic analysis. On the other hand, the digital signal processing of the conventional IEC flickermeter requires the implementation of blocks 1 to 4 independently from the spectral analysis.

4 Conclusions

In this paper, a new analytical estimator for LF in the frequency domain, which is able to take into account also the frequency components neglected by the classical methods proposed in literature, has been proposed. The analytical solutions proposed apply for any generic stationary signal affected by interharmonic distortion. The LF analytical estimator proposed has been applied to numerous numerical case studies with the goal of showing i) the correctness and the improvements of the analytical approach proposed in respect with the other method proposed in literature and ii) the accuracy of the results compared to those obtained by means of the classical IEC flickermeter. The usefulness of the proposed analytical approach is that it can be included in signal processing tools for interharmonic penetration studies for the integration of renewable energy sources in future smart grids.

The main outcomes of the paper are as follows:

- In the presence of interharmonic tones in the frequency range from DC to 15 Hz and from 85 to 100 Hz, the simplified assumptions made by classical methods proposed in literature can lead to very inaccurate results.
- The analytical formulas can be used to perform interharmonic penetration studies in transmission and distribution networks.

Future development of the research will be aimed to generalize the methodology adapted to interharmonic components at frequencies higher than 100 Hz which is proven to affect modern lighting systems different from incandescent bulbs.

5 Appendix A Analytical assessment of $\mathrm{PU}_{1\_\mathrm{AC}}(t)$

With reference to (11), it is possible to demonstrate that the summands of (12) are equal to the following:

$$\begin{aligned} PU_{1\_AC1\_\Delta\omega_1}(t) \cong \frac{H^2|Y_{\Delta\omega_1}|}{2}\{\, & 2|G_{\Delta\omega_1}||G_{2\Delta\omega_1}|a_0 a_{1\_L}^2 a_{1\_U}\cos(\Delta\omega_1 t \\ & +\varphi_{1\_U}-\varphi_1-\angle G_{\Delta\omega_1}+\angle G_{2\Delta\omega_1}+\angle Y_{\Delta\omega_1}) \\ & +2|G_{\Delta\omega_1}||G_{2\Delta\omega_1}|a_0 a_{1\_L} a_{1\_U}^2\cos(\Delta\omega_1 t-\varphi_{1\_L} \\ & +\varphi_1-\angle G_{\Delta\omega_1}+\angle G_{2\Delta\omega_1}+\angle Y_{\Delta\omega_1}) \\ & +|G_{2\omega_1-2\Delta\omega_1}||G_{2\omega_1-\Delta\omega_1}|a_0 a_{1\_L}^3\cos(\Delta\omega_1 t-\varphi_{1\_L} \\ & +\varphi_1-\angle G_{2\omega_1-2\Delta\omega_1}+\angle G_{2\omega_1-\Delta\omega_1}+\angle Y_{\Delta\omega_1})\}, \end{aligned} \tag{23}$$

$$\begin{aligned} \mathrm{PU}_{1\_AC1\_2\Delta\omega}(t) \cong \frac{H^2}{2}|Y_{2\Delta\omega_1}||G_{\Delta\omega_1}|^2 a_0^2[\, & a_{1\_L}^2\cos(2\Delta\omega_1 t-2\varphi_{1\_L} \\ & +2\varphi_1+2\angle G_{\Delta\omega_1}+\angle Y_{2\Delta\omega_1})+a_{1\_U}^2\cos(2\Delta\omega_1 t \\ & +2\varphi_{1\_U}+2\varphi_1-2\angle G_{\Delta\omega_1}+\angle Y_{2\Delta\omega_1}) \\ & +2a_{1\_L}a_{1\_U}\cos(2\Delta\omega_1 t-\varphi_{1\_L}+\varphi_{1\_U}+2\angle G_{\Delta\omega_1} \\ & +\angle Y_{2\Delta\omega_1})], \end{aligned} \tag{24}$$

$$\begin{aligned} \mathrm{PU}_{1\_AC1\_3\Delta\omega_1}(t) \cong H^2|Y_{3\Delta\omega_1}||G_{\Delta\omega_1}||G_{2\Delta\omega_1}|a_0 & \\ \times[a_{1\_L}^2 a_{1\_U}\cos(3\Delta\omega_1 t-2\varphi_{1\_L}+\varphi_{1\_U}-\varphi_1 & \\ +\angle G_{\Delta\omega_1}+\angle G_{2\Delta\omega_1}+\angle Y_{3\Delta\omega_1}) & \\ +a_{1\_L}a_{1\_U}^2\cos(3\Delta\omega_1 t+2\varphi_{1\_U}-\varphi_{1\_L}-\varphi_1 & \\ +\angle G_{\Delta\omega_1}+\angle G_{2\Delta\omega_1}+\angle Y_{3\Delta\omega_1})], & \end{aligned} \tag{25}$$

$$\mathrm{PU}_{1\_\mathrm{AC1}\_4\Delta\omega_1}(t) \cong \frac{H^2}{2}|Y_{4\Delta\omega_1}||G_{2\Delta\omega_1}|^2 a_{1\_\mathrm{L}}^2 a_{1\_\mathrm{U}}^2 \cos(4\Delta\omega_1 t - 2\varphi_{1\_\mathrm{L}} + 2\varphi_{1\_\mathrm{U}} + 2\angle G_{2\Delta\omega_1} + \angle Y_{4\Delta\omega_1}), \tag{26}$$

and that the summands of (13) are equal to the following:

$$\begin{aligned}\mathrm{PU}_{1\_\mathrm{AC2}\_2\omega_1-2\Delta\omega_1}(t) \cong H^2 |Y_{2\omega_1-2\Delta\omega_1}||G_{\Delta\omega_1}||G_{2\omega_1-\Delta\omega_1}|a_0^2 \\ \{a_{1\_\mathrm{L}}^2 \cos[2(\omega_1-\Delta\omega_1)t + 2\varphi_{1\_\mathrm{L}} - \angle G_{\Delta\omega_1} \\ + \angle G_{2\omega_1-\Delta\omega_1} + \angle Y_{2\omega_1-2\Delta\omega_1}] \\ + a_{1\_\mathrm{L}} a_{1\_\mathrm{U}} \cos[2(\omega_1-\Delta\omega_1)t + \varphi_{1\_\mathrm{L}} - \varphi_{1\_\mathrm{U}} \\ + 2\varphi_1 - \angle G_{\Delta\omega_1} + \angle G_{2\omega_1-\Delta\omega_1} + \angle Y_{2\omega_1-2\Delta\omega_1}]\}\end{aligned} \tag{27}$$

$$\mathrm{PU}_{1\_\mathrm{AC2}\_4\omega 1-4\Delta\omega_1}(t) \cong \frac{H^2}{8}|Y_{4\omega_1-4\Delta\omega_1}||G_{2\omega_1-2\Delta\omega_1}|^2 a_{1\_\mathrm{L}}^4 \cos[4(\omega_1-\Delta\omega_1)t + 4\varphi_{1\_\mathrm{L}} + 2\angle G_{2\omega_1-2\Delta\omega_1} + \angle Y_{4\omega_1-4\Delta\omega_1}], \tag{28}$$

6 Appendix B Analytical Assessment of $\mathrm{PU}_{12\_\mathrm{DC}}$

With reference to (15), $\mathrm{PU}_{12\_\mathrm{DC}}$ can be expressed as:

$$\mathrm{PU}_{12\_\mathrm{DC}} = \mathrm{PU}_{12\_\mathrm{DC1}} + \mathrm{PU}_{12\_\mathrm{DC2}}. \tag{29}$$

It is possible to demonstrate that $\mathrm{PU}_{12\_\mathrm{DC1}}$ is equal to:

$$\begin{aligned}\mathrm{PU}_{12\_\mathrm{DC1}} = \frac{1}{2}H^2\{ &|G_{2\omega_1-\Delta\omega_1-\Delta\omega_2}|^2 a_{1\_\mathrm{L}}^2 a_{2\_\mathrm{L}}^2 \\ &+|G_{2\omega_1-\Delta\omega_1+\Delta\omega_2}|^2 a_{1\_\mathrm{L}}^2 a_{2\_\mathrm{U}}^2 \\ &+|G_{2\omega_1+\Delta\omega_1-\Delta\omega_2}|^2 a_{1\_\mathrm{U}}^2 a_{2\_\mathrm{L}}^2 \\ &+|G_{\Delta\omega_1+\Delta\omega_2}|^2 [a_{1\_\mathrm{U}}^2 a_{2\_\mathrm{L}}^2 + a_{1\_\mathrm{L}}^2 a_{2\_\mathrm{U}}^2 \\ &+2a_{1\_\mathrm{L}} a_{1\_\mathrm{U}} a_{2\_\mathrm{L}} a_{2\_\mathrm{U}} \cos(\varphi_{1\_\mathrm{L}} \\ &+\varphi_{1\_\mathrm{U}} - \varphi_{2\_\mathrm{L}} - \varphi_{2\_\mathrm{L}})] \\ &+|G_{\Delta\omega_1-\Delta\omega_2}|^2 [a_{1\_\mathrm{L}}^2 a_{2\_\mathrm{L}}^2 + a_{1\_\mathrm{U}}^2 a_{2\_\mathrm{U}}^2 \\ &+2a_{1\_\mathrm{L}} a_{1\_\mathrm{U}} a_{2\_\mathrm{L}} a_{2\_\mathrm{U}} \cos(\varphi_{1\_\mathrm{L}} \\ &+\varphi_{1\_\mathrm{U}} - \varphi_{2\_\mathrm{L}} - \varphi_{2\_\mathrm{L}})]\},\end{aligned} \tag{30}$$

and that $\mathrm{PU}_{12\_\mathrm{DC2}}$, considering $\Delta\omega_1 > \Delta\omega_2$, assumes different values according to the relationship between $\Delta\omega_1$ and $\Delta\omega_2$:

- For $3\Delta\omega_1 - \Delta\omega_2 = 2\omega_1$, it is equal to:

$$\begin{aligned}\mathrm{PU}_{12\_\mathrm{DC2}} = \frac{1}{2}H^2\{ &|G_{\Delta\omega_1-\Delta\omega_2}|^2 [a_{1\_\mathrm{L}}^3 a_{2\_\mathrm{L}} \cos(3\varphi_{1\_\mathrm{L}} - \varphi_{2\_\mathrm{L}}) \\ &+a_{1\_\mathrm{L}}^2 a_{1\_\mathrm{U}} a_{2\_\mathrm{U}} \cos(2\varphi_{1\_\mathrm{L}} - \varphi_{1\_\mathrm{U}} + \varphi_{2\_\mathrm{U}})] \\ &+2|G_{2\Delta\omega_1}|^2 a_{1\_\mathrm{L}} a_{1\_\mathrm{U}}^2 a_{2\_\mathrm{L}} \cos(-\varphi_{1\_\mathrm{L}} - \varphi_{2\_\mathrm{L}})\},\end{aligned} \tag{31}$$

- For $\Delta\omega_2 + 2\Delta\omega_1 = 2\omega_1$, it is equal to:

$$\begin{aligned}\mathrm{PU}_{12\_\mathrm{DC2}} = \frac{1}{2}H^2\{ &|G_{\Delta\omega_2}|^2 [a_{2\_\mathrm{L}} a_{1\_\mathrm{L}}^2 a \cos(-\varphi_{2\_\mathrm{L}} - 2\varphi_{1\_\mathrm{L}} \\ &+\varphi) + a_{2\_\mathrm{U}} a_{1\_\mathrm{L}}^2 a \cos(\varphi_{2\_\mathrm{U}} - 2\varphi_{1\_\mathrm{L}} + \varphi)] \\ &+2|G_{\Delta\omega_1+\Delta\omega_2}|^2 [a_{1\_\mathrm{L}} a_{1\_\mathrm{U}} a_{2\_\mathrm{L}} a \cos(\varphi_{1\_\mathrm{L}} - \varphi_{1\_\mathrm{U}} \\ &+\varphi_{2\_\mathrm{L}} + \varphi) + a_{1\_\mathrm{L}}^2 a_{2\_\mathrm{U}} a \cos(2\varphi_{1\_\mathrm{L}} - \varphi_{2\_\mathrm{U}} + \varphi)] \\ &+2|G_{\Delta\omega_1}|^2 [a_{2\_\mathrm{L}} a_{1\_\mathrm{L}}^2 a \cos(-\varphi_{2\_\mathrm{L}} - 2\varphi_{1\_\mathrm{L}} + \varphi) \\ &+a_{1\_\mathrm{L}} a_{2\_\mathrm{L}} a_{1\_\mathrm{U}} a \cos(-\varphi_{1\_\mathrm{L}} - \varphi_{2\_\mathrm{L}} + \varphi_{1\_\mathrm{U}} - \varphi)] \\ &+2|G_{2\Delta\omega_1}|^2 a_{2\_\mathrm{L}} a_{1\_\mathrm{L}} a_{1\_\mathrm{U}} a \cos(-\varphi_{2\_\mathrm{L}} - \varphi_{1\_\mathrm{L}} \\ &+\varphi_{1\_\mathrm{U}} - \varphi)\},\end{aligned} \tag{32}$$

- For $\Delta\omega_1 = 2\Delta\omega_2$, it is equal to:

$$\begin{aligned}\mathrm{PU}_{12\_\mathrm{DC2}} = \frac{1}{2}H^2\{ &2|G_{\Delta\omega_1}|^2 [a_{1\_\mathrm{L}} a_{2\_\mathrm{L}} a_{2\_\mathrm{U}} a \cos(-\varphi_{1\_\mathrm{L}} + \varphi_{2\_\mathrm{L}} - \varphi_{2\_\mathrm{U}} \\ &+\varphi) + a_{1\_\mathrm{U}} a_{2\_\mathrm{L}} a_{2\_\mathrm{U}} a \cos(\varphi_{1\_\mathrm{U}} + \varphi_{2\_\mathrm{L}} - \varphi_{2\_\mathrm{U}} - \varphi)] \\ &+2|G_{\Delta\omega_2}|^2 [a_{1\_\mathrm{L}} a_{2\_\mathrm{L}}^2 a \cos(+\varphi_{1\_\mathrm{L}} - 2\varphi_{2\_\mathrm{L}} + \varphi) \\ &+a_{1\_\mathrm{U}} a_{2\_\mathrm{L}} a_{2\_\mathrm{U}} a \cos(-\varphi_{1\_\mathrm{U}} - \varphi_{2\_\mathrm{L}} + \varphi_{2\_\mathrm{U}} \\ &+\varphi) + a_{1\_\mathrm{L}} a_{2\_\mathrm{L}} a_{2\_\mathrm{U}} a \cos(\varphi_{1\_\mathrm{L}} - \varphi_{2\_\mathrm{L}} + \varphi_{2\_\mathrm{U}} - \varphi) \\ &+a_{1\_\mathrm{U}} a_{2\_\mathrm{U}}^2 a \cos(-\varphi_{1\_\mathrm{U}} + 2\varphi_{2\_\mathrm{U}} - \varphi)] \\ &+2|G_{2\omega_1-\Delta\omega_1+\Delta\omega_2}|^2 a_{1\_\mathrm{L}} a_{2\_\mathrm{L}} a_{2\_\mathrm{U}} a \cos(-\varphi_{1\_\mathrm{L}} \\ &+\varphi_{2\_\mathrm{L}} - \varphi_{2\_\mathrm{U}} + \varphi) + |G_{2\omega_1-2\Delta\omega_2}|^2 a_{1\_\mathrm{L}} a_{2\_\mathrm{L}}^2 a \\ &\cos(-\varphi_{1\_\mathrm{L}} + 2\varphi_{2\_\mathrm{L}} - \varphi)\}.\end{aligned} \tag{33}$$

Competing interests
The authors declare that they have no competing interests.

Acknowledgements
The research activity discussed in this paper has been partially supported by the Project PON01_02582 "Command, control, protection and supervision integrated system for production, transmission and distribution (ColAdMin integrated SCADA) of renewable and non renewable electrical energy, with field-device-interface, for rational use of electrical power" funded by the Italian Ministry for the Instruction, University and Research.

Received: 15 December 2014 Accepted: 16 February 2015
Published online: 24 March 2015

References

1. IEEE Task, Force on harmonics modeling and simulation, interharmonics: theory and modeling. IEEE Trans. Power Deliv. **22**(4), 2335–2348 (2007). doi:10.1109/TPWRD.2007.905505
2. IEC Standard 61000-4-15. Flickermeter—functional and design specifications (IEC, Geneva, Switzerland, Edition 2.0, 2010-07)
3. R Langella, A Testa, Amplitude and phase modulation effects of waveform distortion in power systems. J. Electrical Power Qual. Util. **XIII**(1), 25–32 (2007)
4. D Gallo, R Langella, A Testa, *Light Flicker Prediction Based on Voltage Spectral Analysis* (Paper presented at the IEEE Porto Power Tech Conference, Porto, Portogallo, 2001), pp. 10–13
5. R Langella, A Testa, Power System Subharmonics, ed. by IEEE (Paper invited at the IEEE Power Engineering Society General Meeting 2005, S. Francisco, USAm, 2005)
6. T Keppler, NR Watson, S Chen, J Arrilaga, Digital flickermeter realisations in the time and frequency domains, ed. by Australasian Committee for Power Engineering (Paper presented at the Australasian Power Engineering Conference, Perth, Australia, September, 2001)

7. A Hernandez, JG Mayordomo, R Asensi, LF Beites, A new frequency domain approach for flicker evaluation of arc furnaces. IEEE Trans. Power Deliv. **18**(2), 631–638 (2003). doi:10.1109/TPWRD.2003.809733
8. CJ Wu, TH Fu, Effective voltage flicker calculation algorithm using indirect demodulation method. IEE P-Gener. Transm. D. **150**(4), 493–500 (2003). doi:10.1049/ip-gtd:20030302
9. T Keppler, NR Watson, J Arrilaga, S Chen, Theoretical assessment of light flicker caused by sub- and interharmonic frequencies. IEEE Trans. Power Deliv. **18**(1), 329–333 (2003). doi:10.1109/TPWRD.2002.806690
10. D Gallo, R Langella, C Landi, A Testa, On the use of the flickermeter to limit low-frequency interharmonic voltages. IEEE Trans. Power Deliv. **23**(4), 1720–1727 (2008). doi:10.1109/TPWRD.2008.2002842
11. N Kose, O Salor, New spectral decomposition based approach for flicker evaluation of electric arc furnaces. IET Gener. Transm. Dis. **3**(4), 393–411 (2009). doi:10.1049/iet-gtd.2008.0479
12. GW Chang, C Cheng-I, H Ya-Lun, A digital implementation of flickermeter in the hybrid time and frequency domains. IEEE Trans. Power Deliv. **24**(3), 1475–1482 (2009). doi:10.1109/TPWRD.2009.2022673
13. A Hernández, JG Mayordomo, R Asensi, LF Beites, A method based on interharmonics for flicker propagation applied to arc furnaces. IEEE Trans. Power Deliv. **20**(3), 2334–2342 (2005). doi:10.1109/TPWRD.2005.848677
14. IEC standard 61000-4-7: General guide on harmonics and interharmonics measurements, for power supply systems and equipment connected thereto (IEC, Geneva, Switzerland, Edition 2.0, 2002-08)
15. K Yang, MHJ Bollen, EO Anders Larsson, M Wahlberg, Measurements of harmonic emission versus active power from wind turbines. Electr. Pow. Syst. Res. **108**, 304–314 (2014). doi:10.1016/j.epsr.2013.11.025
16. F De Rosa, R Langella, A Sollazzo, A Testa, On the interharmonic components generated by adjustable speed drives. IEEE Trans. Power Deliv. **20**(4), 2535–2543 (2005). doi:10.1109/TPWRD.2005.852313
17. R Carbone, F De Rosa, R Langella, A Testa, A new approach for the computation of harmonics and interharmonics produced by line-commutated AC/DC/AC converters. IEEE Trans. Power Deliv. **20**(3), 2227–2234 (2005). doi:10.1109/TPWRD.2005.848448
18. R Langella, A Sollazzo, A Testa, A new approach for the computation of harmonics and interharmonics produced by AC/DC/AC conversion systems with PWM inverters. Eur. T. Electr. Power **20**(1), 68–82 (2010). doi:10.1002/etep.400